CHALMERS
UNIVERSITY OF TECHNOLOGY

Model-based estimation of rail roughness from axle box acceleration

Applied Acoustics 193 (2022) 108760

Contents lists available at ScienceDirect

Applied Acoustics

journal homepage: www.elsevier.com/locate/apacoust

Model-based estimation of rail roughness from axle box acceleration

Astrid Pieringer *, Wolfgang Kropp

Division of Applied Acoustics, Chalmers University of Technology, SE-41296 Göteborg, Sweden

ARTICLE INFO

Article history:
Received 31 August 2021
Received in revised form 30 January 2022
Accepted 24 March 2022
Available online 7 April 2022

Keywords:
Axle box acceleration
Rail roughness
Acoustic monitoring
Wheel/rail interaction
Time domain
Source identification

ABSTRACT

Monitoring rail roughness in the railway network allows directing grinding actions to where they are needed to reduce rolling noise and large wheel/rail forces. To be able to measure rail roughness on a large scale, indirect measurements onboard railway vehicles have to be carried out. Existing methods use either axle box acceleration (ABA) or under-coach noise measurements to monitor the rail roughness indirectly. The two main challenges with rail roughness estimation from vibroacoustic signals measured onboard vehicles are to separate wheel and rail roughness and to take into account varying track dynamics in the railway network. Both questions have not yet been addressed sufficiently.

In this paper, an enhanced method for estimating rail roughness from ABA is presented. In contrast to all existing methods in the literature, the presented method operates in the time domain. A time-domain method has the advantage that the spatial variations of roughness become visible and paves the way for the detection of localized defects such as squats or deteriorated welds. The method is based on a previously developed time-domain model for high-frequency wheel/rail interaction and estimates the time series of the roughness from the time series of ABA. In a first step, the time series of the contact force is calculated from the axle box acceleration using a Least Mean Square algorithm for source identification. In a second step, the combined wheel/rail roughness is obtained from the contact force based on a nonlinear Hertzian contact model and a convolutional approach to determine wheel and rail displacement. Separation of wheel and rail roughness is possible by cycle-averaging the contact force over a distance corresponding to the wheel perimeter and performing the second step separately for the part of the contact force originating from the wheel and the rail roughness, respectively.

The method was tested for simulated ABA obtained from measured wheel and rail roughness. In the relevant wavelength range from 0.5 m to 5 mm, the rail roughness could be estimated with good accuracy for known track dynamics. Overall, deviations in 1/3-octave bands between estimated and actual roughness were below 1 dB. Only for low rail roughness, higher deviations of less than 2.6 dB occurred around the pinned-pinned resonance frequency. Uncertainties in the track parameters affect the roughness estimation, where the most critical parameter is the rail pad stiffness. A deviation of 20% in rail pad stiffness leads to deviations in the rail roughness of up to 3.5 dB in single 1/3-octave bands. The results illustrate the need to extend the method for the simultaneous extraction of track parameters and roughness from measured axle box acceleration.

1. Introduction

Infrastructure managers need to have control over the acoustic quality of the tracks in their network. This concerns predominantly knowledge about the rail roughness that, together with the wheel roughness, generates rolling noise during train passage. The combined wheel/rail roughness excites vibrations of track and wheel in the form of a vertical relative motion. In consequence, the wheelset, the rail, and the sleepers radiate noise [1]. Monitoring rail roughness on a large scale allows directing grinding actions to where they are needed to reduce rolling noise and large wheel/rail forces. Such a condition-based maintenance strategy may lead to reduced costs and higher system reliability in comparison to traditional scheduled maintenance.

Rail roughness can be measured directly. Existing measurement devices include beams mounted above the rail, which scan the rail roughness on a short distance of typically 1.2 m, and trolleys pushed along the railhead, which use accelerometers to measure the roughness [1]. Such direct measurement procedures are relatively slow and laborious and require access to the track that has to be closed for train operation. Therefore only short sections of

* Corresponding author.
E-mail address: astrid.pieringer@chalmers.se (A. Pieringer).

https://doi.org/10.1016/j.apacoust.2022.108760
0003-682X/

the track can be measured directly, and these procedures are not suitable for assessing the acoustic track quality of larger sections of the railway network.

To overcome the shortcomings of direct measurements, a number of track providers have started to use measurements either with specially equipped wagons or even with equipment added to regular traffic vehicles. Different methods have been developed using either axle box acceleration (ABA) [2–6], or under-coach noise measurements [7–11], or a combination of both [12,13] to monitor the rail roughness indirectly. The measured acceleration or sound pressure has to be transformed back to the roughness. This is generally done in the frequency domain by using a transfer function that depends both on wheelset and track dynamics. The roughness obtained is the combined wheel/rail roughness.

The two main challenges with rail roughness estimation from vibroacoustic signals measured onboard vehicles are to separate wheel and rail roughness and to take into account varying track dynamics in the railway network. In a recent review paper, Pallas et al. [14] identify three main approaches to separate wheel and rail roughness. A first approach is to use smooth wheels, which puts high constraints on the braking mode of the wheels and requires regular wheel grinding. Smooth wheels are easiest achieved using unbraked wheels, as implemented in DB's noise measurement car [7]. A second approach is to measure wheel roughness directly and remove the wheel contribution from the spectrum of combined roughness. This method gives only accurate results for the rail roughness if the wheel roughness is lower than the rail roughness. Another problem is that the wheel roughness has to be measured often enough since it changes with time due to wear of the wheel surface. A third approach, first proposed by Németh and Schleinzer [3], is based on synchronous spatial averaging (also called cycle-averaging) of the sensor signal and exploits the fact that the wheel roughness repeats with every wheel rotation while the rail roughness has a random character. This approach "consists in slicing the sensor signal in sections of the duration of one wheel rotation and in averaging them to bring out the deterministic wheel contribution while removing the random rail input" [14]. This method to estimate the rail roughness works well even if the wheel roughness is higher than the rail roughness but relies on perfect periodicity of the wheel roughness. Pallas et al. [14] demonstrate the sensitivity of the method to lateral motion of the contact point during train operation.

The problem of taking into account the track dynamics has not yet been addressed sufficiently. It is either ignored or addressed by calibrating the measurement system on a reference site where direct roughness measurements are carried out. Large errors may occur when the system is applied on track with dynamic characteristics different from the reference track [5,10].

Chartrain [11] proposed a methodology to assess both the level of rail roughness and the dynamic behaviour of the track by onboard sound measurements. The methodology combines sound measurements close to a wheel and close to the rail with calculations with frequency-domain models for wheel/rail interaction and wheel and track radiation. The identification of the dynamic behaviour of the track is based on the detection of rail pad stiffness and sleeper types by means of acoustic signatures of the track radiation. Due to the used simplified submodels, the proposed methodology is, however, not valid in the complete wavelength range of interest.

Based on idealized vehicle and track modelling, Carrigan and Talbot [6] showed that it is possible to extract both track foundation parameters and rail roughness spectra from simulated ABA data. They used cycle-averaging to separate wheel and rail roughness. So far, the method has not been tested on real measurement data of ABA and roughness.

All the above methods for indirect roughness measurement work with transfer functions in the frequency domain. In this paper, a method is developed which estimates the time series of the roughness from the time series of the axle box acceleration. A time-domain method has the advantage that the spatial variations of the roughness become visible. It should also be possible to discover localized defects such as squats or deteriorated welds. The method is based on the time-domain model WERAN (WhEel/RAil Noise) for wheel/rail interaction and noise developed at Chalmers Applied Acoustics [15], which is shortly presented in Section 2. In a first step outlined in Section 3, the time series of the contact force is calculated from the axle box acceleration using a Least Mean Square (LMS) algorithm [16]. In a second step, the combined wheel/rail roughness is obtained from the contact force based on non-linear Hertzian contact and a convolutional approach to determine wheel and rail displacement, see Section 4. In Section 5, separation of wheel and rail roughness is accomplished by cycle-averaging the contact force over a distance corresponding to the wheel perimeter and performing the second step separately for the part of the contact force originating from the wheel and the rail roughness, respectively. In this paper, indirect rail roughness measurement is demonstrated for known track dynamics. The influence of uncertainties in the track parameters on the roughness estimation is assessed in Section 6. In future work, the method will be extended to simultaneously extract track dynamics and rail roughness in a similar way as proposed in [6].

The aim of this paper is to present a new measurement method for rail roughness and demonstrate its functioning in a simulated environment using detailed wheelset, track and contact models. Before taking the step to test the method on measurement data, it will be necessary to evaluate the effect of possible error sources and uncertainties present in real context on the roughness estimation using the simulated environment. This future work includes investigating the consequences of e.g. errors in calibration of the wheelset model and the lateral motion of the contact point on wheel and rail.

2. The model WERAN

The methodology to estimate rail roughness from ABA presented in this paper builds on the non-linear time-domain model WERAN [15,17] that has been developed to calculate high-frequency wheel/rail interaction and noise.

2.1. Overview of WERAN

WERAN includes a detailed three-dimensional submodel of the wheel/rail contact based on Kalker's variational method [18], considering both normal and tangential interaction. Only normal interaction is included here since this is considered sufficient in the context of roughness excitation. The normal contact model takes as input the complete three-dimensional roughness profile of the wheel and rail. This usually is available in the form of a few measured parallel longitudinal roughness lines. To get the required lateral roughness resolution, these lines have to be interpolated in the lateral direction. While WERAN has the capability to consider two wheel/rail contacts (one on each wheel) and their coupling via the wheelset axle and the sleepers [19] as long as suitable wheelset and track submodels are used, only one wheel/rail contact has been included in this paper.

WERAN employs a Green's function approach, which leads to a computationally efficient model allowing for large parameter studies. Vehicle and track are represented by Green's functions (impulse response functions) that are pre-calculated from the receptances at the contact point by inverse Fourier transform.

Instead of performing a time integration, the wheel and rail displacements $\xi_w(t)$ and $\xi_r(t)$ are obtained by convolving the time series of contact forces $F(t)$ with the Green's functions:

$$\xi_w(t) = -\int_0^t F(\tau) g_w(t-\tau)\,\mathrm{d}\tau + \xi_s(P), \tag{1}$$

$$\xi_r(t) = \int_0^t F(\tau) g_{r,v}^{v\tau}(t-\tau)\,\mathrm{d}\tau. \tag{2}$$

The function $g_w(t)$ is the Green's function of the wheel in the contact point and $g_{r,v}^{x_0}(t)$ is a moving Green's function of the track that takes into account the motion of the contact point along the rail. For excitation of the rail at the position x_0 at time $t_0 = 0$, the function $g_{r,v}^{x_0}(t)$ describes the displacement response of the rail at a point moving at train speed v away from the excitation. The train speed v is assumed constant. The expression $\xi_s(P)$ is the position of the primary suspension corresponding to the static preload P.

2.2. Application case

For the simulations in this paper, WERAN was adapted to the conditions during a field measurement campaign from the innovation project Roll2Rail [20], which took place in June 2016 at the highspeed line Munich – Augsburg, close to the village Haspelmoor about 38 km northwest of Munich. The track at the test site consisted of rails with profile UIC60 E2 on monobloc concrete sleepers in ballast. Pass-by measurements were carried out with DB's noise measurement car Schallmesswagen (SMW) [7]. The purpose of the measurements had been to validate different methods to separate the wheel and rail contribution to the rolling noise. Before the pass-by measurements, track decay rate (TDR), wheel receptances, rail roughness (on one line), and wheel roughness of wheels of the measurement bogie of the SMW (on three parallel lines) had been measured.

2.3. Track model

The track model used is the finite element (FE) model accounting for discrete supports presented by Nielsen in [21]. The model comprises one rail represented by Rayleigh–Timoshenko beam elements on discrete supports consisting of rail pads and sleepers on ballast. The track parameters are given in Table 1.

Stiffness and damping parameters of the rail support have been identified by adapting simulated track receptance and TDR to the measurements of these quantities. Fig. 1 (*left*) shows the simulated vertical point receptance of the track for excitation on the rail above a sleeper and for excitation at midspan between two sleepers. The two receptances differ by the peak of the pinned–pinned resonance occurring at 1071 Hz. The corresponding moving Green's functions of the track for a train speed of 80 km/h are seen in Fig. 1 (*right*). For comparison, the measured vertical point receptance of the track is also given in Fig. 1 (*left*). It agrees well with its simulated counterpart, except at the antiresonance at 2788 Hz, which is shifted upwards in frequency in the simulation.

Table 1
Parameters of the track model.

Bending stiffness of rail (Nm^2)	EI	$6.3 \cdot 10^6$
Shear stiffness of rail (N)	kGA	$250 \cdot 10^6$
Rail mass per unit length (kg/m)	$m\prime$	60
Rail head radius (m)	R_r	0.30
Sleeper spacing (m)	L_s	0.60
Rail pad stiffness (N/m)	k_p	$114 \cdot 10^6$
Rail pad damping (Ns/m)	c_p	$5 \cdot 10^3$
Sleeper mass (half) (kg)	m_s	140
Ballast stiffness per half sleeper (N/m)	k_b	$75 \cdot 10^6$
Ballast damping per half sleeper (Ns/m)	c_b	$150 \cdot 10^3$
Viscous bending damping of rail (Nm^{2}s)	c_r	2.4

2.4. Wheelset model

The vehicle model includes a complete wheelset of the SMW comprising the axle, two wheels of type BA093, two brake disks, and the primary suspension [22]. All vehicle components above the primary suspension are represented as a static preload P. The parameters of the flexible wheelset model are listed in Table 2.

The wheelset was modelled using commercial finite element (FE) software. The eigenfrequencies and eigenmodes have been calculated up to 10 kHz with this undamped FE model. The modal damping was obtained from the measured radial and axial wheel receptances at the contact. Modes that could not be identified in the measurements were assigned the approximate damping values for rolling noise proposed by Thompson [1]. The measured receptances were also used to update the eigenfrequencies while the eigenmodes were not changed. From this modal basis, the Green's functions of the wheelset were calculated. The measured and simulated radial (vertical) point receptances of the wheelset at the contact point on the wheel and the corresponding simulated Green's function are shown in Fig. 2. The described adaption of the FE model to the measurements leads to a very good agreement between measured and simulated receptances at the main resonances dominating the wheel response, while differences at minor resonances and anti-resonances remain.

The axle boxes of the wheelset were not modelled. Instead, it is assumed that the acceleration at a point on the axle 8 cm from the axle end approximately corresponds to the axle box acceleration. As a measurement of transfer function from the contact point on the wheel tread to the axle box was not available, the validity of this assumption could not be verified. This does, however, not compromise the proposed method for indirect roughness measurement. In a practical implementation of the method, care needs to be taken to calibrate the transfer function from the contact to the axle box [13], which might involve an extension of the model to include bearing and axle box. The simulated transfer accelerance from the contact point on the wheel tread to the axle box and the corresponding Green's function $g_{w,aba}$ are depicted in Fig. 3.

2.5. Roughness data

For the simulations in this paper, the measured roughness of one of the wheels in the measurement bogie of the SMW was used. This roughness had been measured on three traces (0 mm, +10 mm, −10 mm) with a longitudinal resolution of 0.8 mm and was interpolated to obtain a 3D roughness profile with a longitudinal and lateral resolution of 1 mm. The rail roughness had been measured with a trolley over a length of 157 m on the two rails at the test site with a longitudinal resolution of 1 mm, but only in one trace on each rail. The spatial raw data was only available band-pass filtered from 4 to 500 mm. To construct a 3D roughness profile needed as input to the simulations, eleven suitable 20 m-long pieces of the roughness (not featuring localized defects or any other large singular peaks) were placed beside each other at a distance of 2 mm, see Fig. 4, and then interpolated to 1 mm lateral resolution. The resulting rail roughness profile has very low lateral correlation at all wavelengths, which is what is expected in the absence of corrugation. To obtain a roughness profile longer than 20 m, the original profile was prolonged by alternately adding a mirrored version of the profile and the original profile.

Spike removal according to EN15610 [23] has been carried out for both wheel and rail roughness. Narrow upward spikes in the

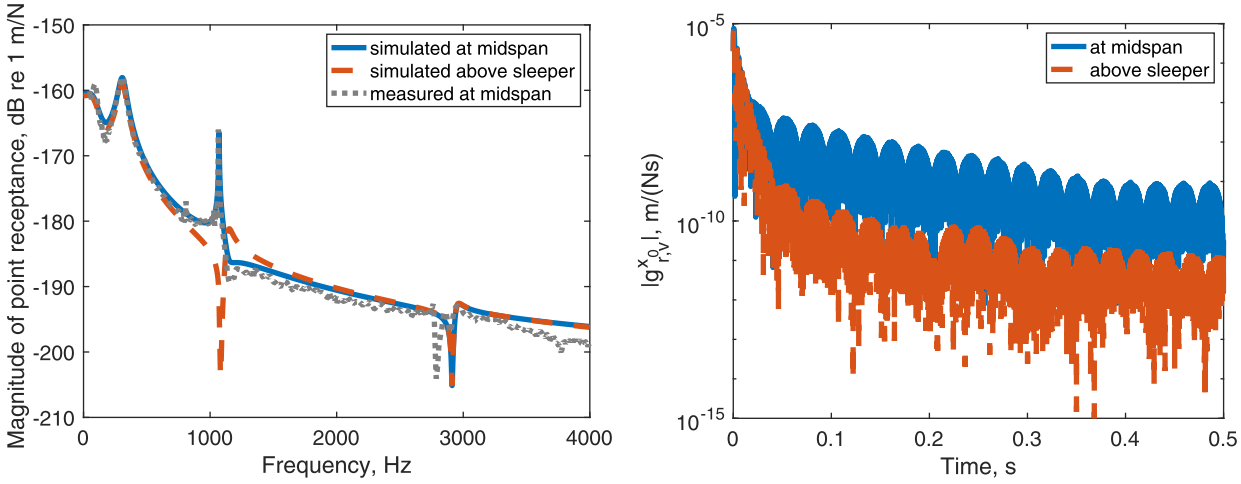

Fig. 1. Simulated vertical point receptance of the track at the contact point on the rail at midspan and above a sleeper in comparison to the measured receptance at midspan (*left*) and corresponding simulated moving Green's functions $g^{x_0}_{r,v}$ at 80 km/h (*right*).

Table 2
Parameters of the wheelset model.

Stiffness of primary suspension (N/m)	k_s	$1.60 \cdot 10^6$
Damping of primary suspension (Ns/m)	c_s	$12.0 \cdot 10^3$
Radius (reprofiled wheel) (m)	R_w	0.469
Static preload (N)	P	$55.2 \cdot 10^3$
Young's modulus (Pa)	E	$206 \cdot 10^9$
Density (kg/m^3)	ρ	7810

roughness are interpreted as the presence of small particles of foreign matter, which have to be removed to obtain the correct roughness profile experienced by the wheel/rail contact. Curvature processing according to EN15610 has *not* been conducted since the curvature of the wheel is taken into account in the 3D contact model.

An autospectrum of wheel and rail roughness has been calculated separately for each roughness line and then energetically averaged over the different lines, see Fig. 5 (*left*). The corresponding 1/3-octave band spectra are shown in Fig. 5 (*right*) in comparison to the ISO 3095:2013 limit for rail roughness applying during vehicle type testing [24]. Wheel and rail roughness have about the same order of magnitude for wavelengths from 300 mm to 22 mm, but below 22 mm the wheel roughness is dominating. The equivalent wheel and rail roughness obtained by processing the roughness with the 3D contact filter described in Section 4 is also depicted in Fig. 5 (*right*). Three effects are taken into account during the contact filtering: First, roughness components of wavelengths that are in the order of or shorter than the length of the contact area in the rolling direction do not excite the system as effectively as roughness components of longer wavelengths [25,26], an effect known as the actual contact filter effect. Second, the excitation of the wheel/rail system is greatest when the roughness is strongly correlated across the width of the contact patch in the lateral direction and progressively decreases as the roughness becomes uncorrelated. Third, the curvature of the wheel is taken into account. Due to the finite curvature of the wheel, it will not 'see' parts of the roughness profile (e.g. pits) when the wheel runs along the rail. In Fig. 5 (*right*), the contact filter effect is clearly noticeable for wavelength up to 30 mm, which is between three and four times the length of the contact patch (the latter being 9 mm assuming cylindrical wheel and rail profiles). Since the constructed rail roughness profile is highly uncorrelated in the lateral direction, the equivalent rail roughness is below the unfiltered rail roughness in the complete wavelength range. This is not the case for the wheel roughness. As a consequence, the equivalent rail

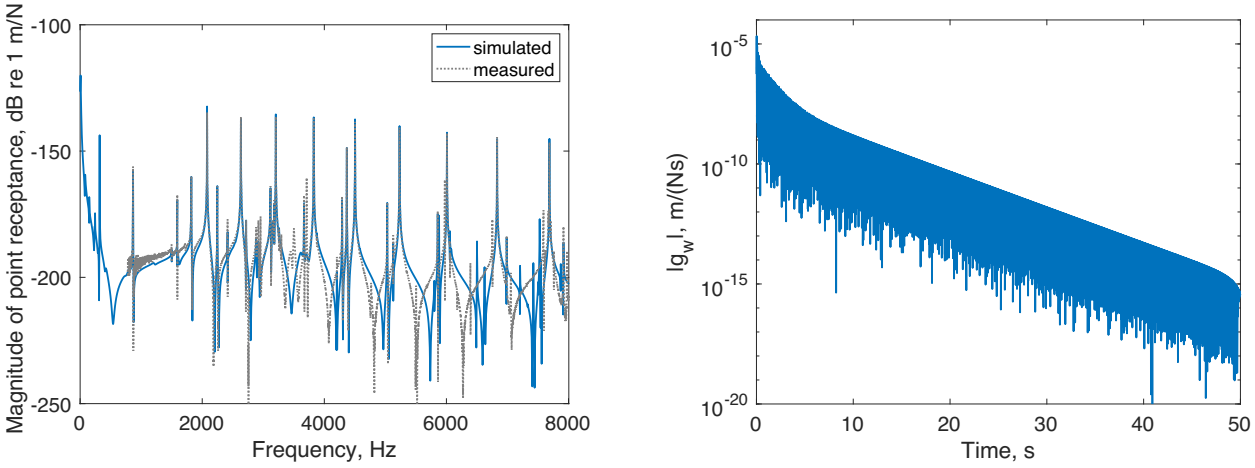

Fig. 2. Simulated radial point receptance of the wheelset at the contact point on the wheel tread in comparison to the measurement (*left*) and corresponding simulated Green's function g_w (*right*).

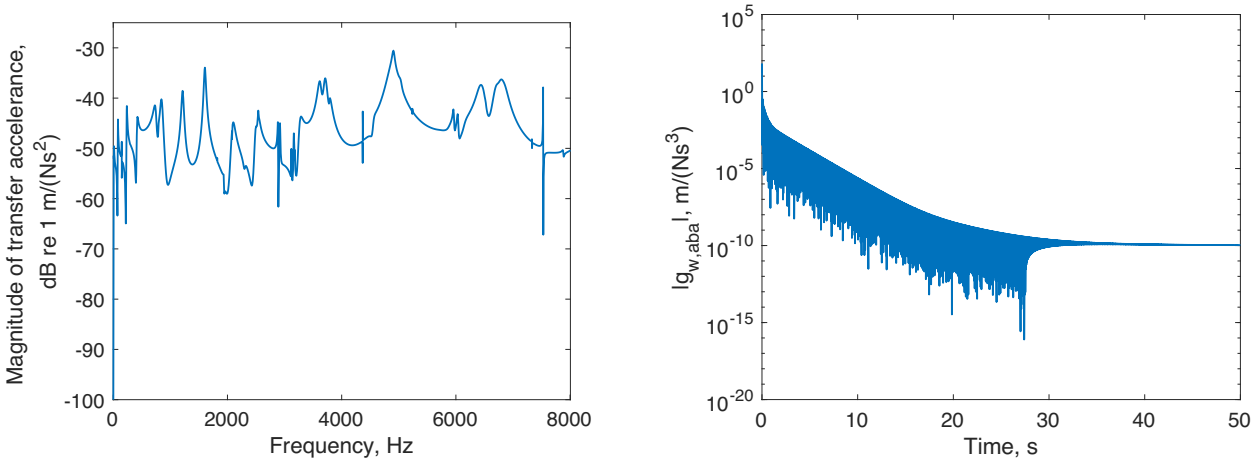

Fig. 3. Transfer accelerance from contact point on the wheel tread to axle box (*left*) and corresponding Green's function $g_{w,aba}$ (*right*).

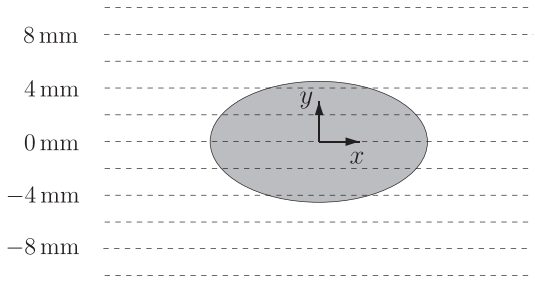

Fig. 4. Longitudinal roughness lines building the rail roughness profile and nominal contact area. The x-direction is the rolling (longitudinal) direction and the y-direction is the lateral direction.

roughness is below the equivalent wheel roughness in all 1/3-octave bands, except one (at 400 mm).

2.6. The nominal case

The described wheel and rail roughness profiles were used as input to WERAN to calculate the time series of the normal contact force for a train speed v of 80 km/h with temporal resolution $\Delta t = \Delta x / v = 4.5 \cdot 10^{-5}$ s. The ABA signal is determined in a post-processing step by convolving the contact forces with the Green's function $g_{w,aba}$ calculated from the transfer accelerance between the contact point on the wheel tread and the axle box. The autospectrum of the obtained ABA signal is given in Fig. 6. The time series of the ABA signal of this nominal case is used in the following sections as the starting point for roughness estimation and separation.

3. Estimation of the contact force

The first step in the roughness estimation from ABA is the estimation of the contact force. The task is to identify the time series of the wheel/rail contact forces that leads to the given time series of ABA. The transfer function from source (contact force) to receiver (ABA) is known in terms of the impulse response function $g_{w,aba}$. The identification of the contact force is thus an inverse problem. In [27], Kropp and Larsson proposed a method for source identification in the time domain by applying a Least Mean Square (LMS) algorithm. An advantage of this algorithm is that it does not require a matrix inversion in contrast to many frequency domain methods applied to solve inverse problems. Therefore, the solution is more robust in the case of low signal-to-noise ratio and ill-conditioned systems [28]. Originally, the LMS algorithm has been

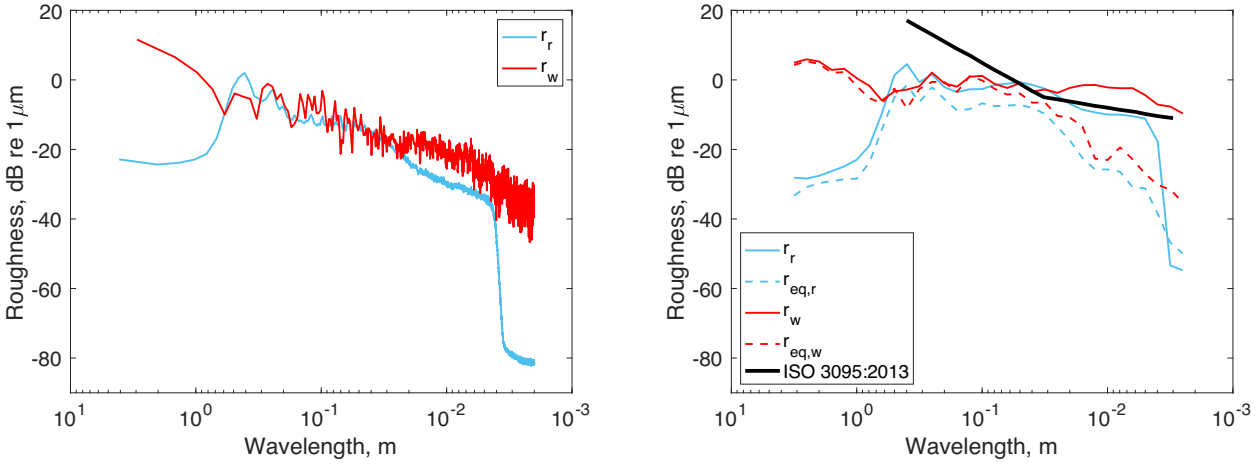

Fig. 5. Autospectra of rail and wheel roughness r_r and r_w averaged over 19 parallel roughness lines (*left*) and corresponding 1/3-octave band spectra in comparison to 1/3-octave band spectra of the equivalent rail and wheel roughness $r_{eq,r}$ and $r_{eq,w}$ obtained from the 3D contact filter (*right*).

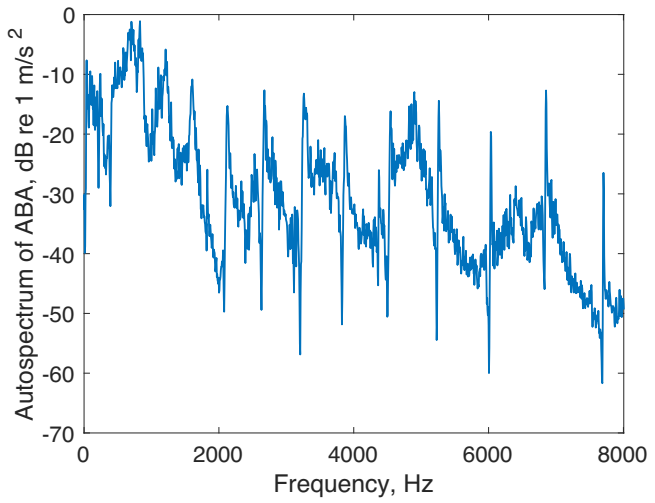

Fig. 6. Autospectrum of ABA.

developed by Widrow and Hoff [16] for the design of digital filters. The method by Kropp and Larsson is applied here.

The LMS algorithm determines the source signal $F_{\text{est}}(n)$ at time step n in such a way that the mean square of the error between the known receiver signal $a(n)$ and the estimated receiver signal $a_{\text{est}}(n)$ is minimized, see Fig. 7.

The error $e(n)$ at time step n is

$$e(n) = a(n) - a_{\text{est}}(n) = a(n) - \sum_{i=0}^{I-1} F_{\text{est}}(n-i)\, g_{\text{w,aba}}(i), \tag{3}$$

where the summation is a convolution between the estimated force and the impulse response function that has a finite number of I values. The values of F_{est} are obtained from

$$\mathbf{F}_{\text{est,new}}(n) = \mathbf{F}_{\text{est,old}}(n) + \alpha\, e(n)\, \mathbf{g}_{\text{w,aba}} \quad \text{for } I \leqslant n < N, \tag{4}$$

where $\mathbf{F}_{\text{est}}(n)$ is the vector

$$[F_{\text{est}}(n), F_{\text{est}}(n-1), \ldots, F_{\text{est}}(n-I+1)], \tag{5}$$

and $\mathbf{g}_{\text{w,aba}}$ is the vector

$$[g_{\text{w,aba}}(0), g_{\text{w,aba}}(1), \ldots, g_{\text{w,aba}}(I-1)]. \tag{6}$$

N is the number of values in a (and F_{est}), and α is a weighting factor determining the step size in the iterative process. After stepping through all n, the process in Eq. (4) is repeated starting from the values $\mathbf{F}_{\text{est}}(n)$ from the previous iteration as many times as necessary to reach a sufficiently small mean square error. The first $2I$ values of the signal F_{est} cannot be reconstructed correctly and will always be erroneous.

The described LMS algorithm is applied for source reconstruction on the ABA signal calculated with WERAN. The length N of the ABA signal is 141600 samples. For the source reconstruction, the impulse response function $g_{\text{w,aba}}$ is approximated by its first

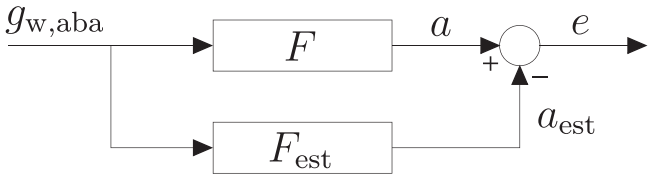

Fig. 7. Process for source identification.

10000 values (i.e. $I = 10000$) corresponding to 0.45 s, which showed to be sufficient since $g_{\text{w,aba}}$ has already decreased by almost 70 dB in this time period. Fig. 8 (*left*) shows a section of the reconstructed contact force F_{est} after 2000 iterations in comparison to the original signal F. The estimation error for the complete signal is given in Fig. 8 (*right*). The estimated signal is erroneous up to $2I$, but due to the rapid decrease of $g_{\text{w,aba}}$ the error decreases rapidly after I samples. The autospectra of estimated and original contact force are compared in Fig. 9. The autospectra have been calculated for the signal range from $2I$ to $N - I$ using a block length of 4096 samples. The estimation error is small in the complete frequency range. The peaks in Fig. 9 (*right*) that are still small errors below 0.5 dB occur at discrete frequencies that correspond to more lightly damped wheelset modes visible in the transfer function in Fig. 3 (*left*) as sharp but not necessarily high peaks.

4. Estimation of the combined wheel/rail roughness

The second step to obtain the roughness from ABA is to calculate the time series of the combined wheel/rail roughness from the time series of the estimated contact forces. This is achieved by employing a non-linear Hertzian contact model combined with the convolutional approach to determine wheel and rail displacement implemented in WERAN.

4.1. Procedure to calculate the combined wheel/rail roughness from the contact forces

Hertzian contact [29] gives the following relation between the normal contact force F and the approach of distant points (i.e. the compression of the contact spring) δ:

$$F(\delta) = C_{\text{h}}\, \delta^{\frac{3}{2}}. \tag{7}$$

The factor C_{h} is a function only of the principal relative radii of curvature and the material parameters. For the parameters used here, C_{h} is $9.459 \cdot 10^{10}\,\text{kg}/(\text{s}^2\text{m}^{0.5})$. The approach of distant points is obtained from wheel and rail displacements and roughness according to

$$\delta(x) = \xi_{\text{w}}(x) - \xi_{\text{r}}(x) + r_{\text{eq}}(x). \tag{8}$$

It follows from Eqs. (7) and (8) that the roughness can be calculated from the estimated contact force as

$$r_{\text{eq, est}}(x) = \left(\frac{F_{\text{est}}(x)}{C_{\text{h}}}\right)^{\frac{2}{3}} - \xi_{\text{w}}(x) + \xi_{\text{r}}(x). \tag{9}$$

Wheel and rail displacement are determined by convolving the contact force with the wheel and rail Green's functions, respectively, as shown in Eqs. (1) and (2).

4.2. 3D contact filter

The roughness obtained from Eq. (9) is not the 3D profile of roughness raw data but an equivalent combined wheel/rail roughness. The same type of roughness is obtained when applying a 3D contact filter to the roughness raw data. Such a contact filter can be constructed from Kalker's algorithm NORM [18], which is implemented in WERAN, as explained in the following.

NORM relies on the assumption that both wheel and rail can be locally approximated by elastic half-spaces. The potential contact area is divided into N_e rectangular elements of dimensions Δx and Δy in longitudinal and lateral directions, respectively. The relation between the combined normal surface displacement $\mathbf{u}$ and contact pressure $\mathbf{p}$ in all elements of the potential contact area is

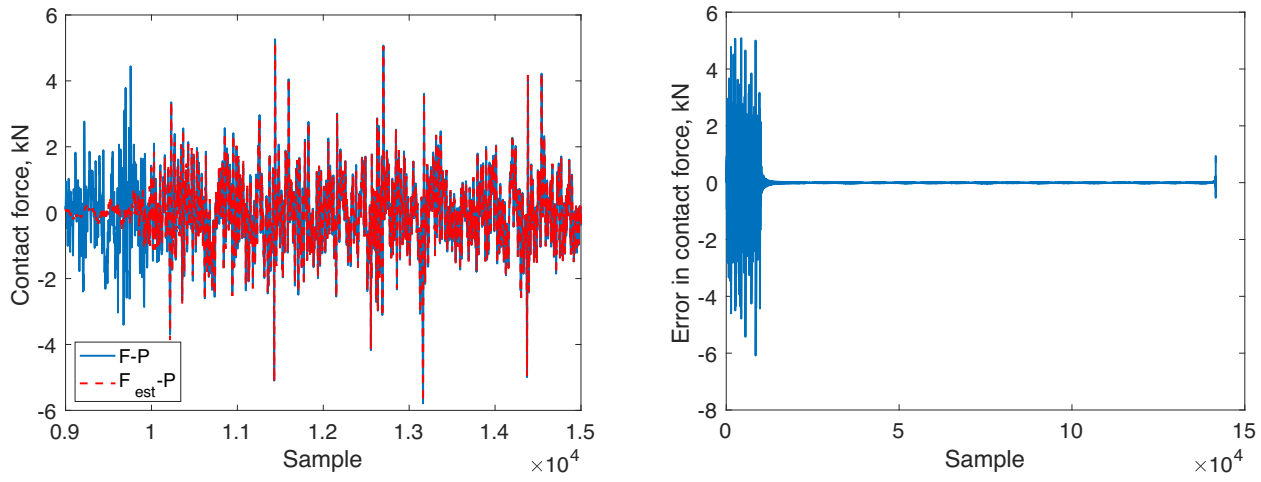

Fig. 8. Time series of the original dynamic contact force $F-P$ in comparison to the estimated force $F_{\text{est}}-P$ (*left*) and error $F_{\text{est}}-F$ (*right*).

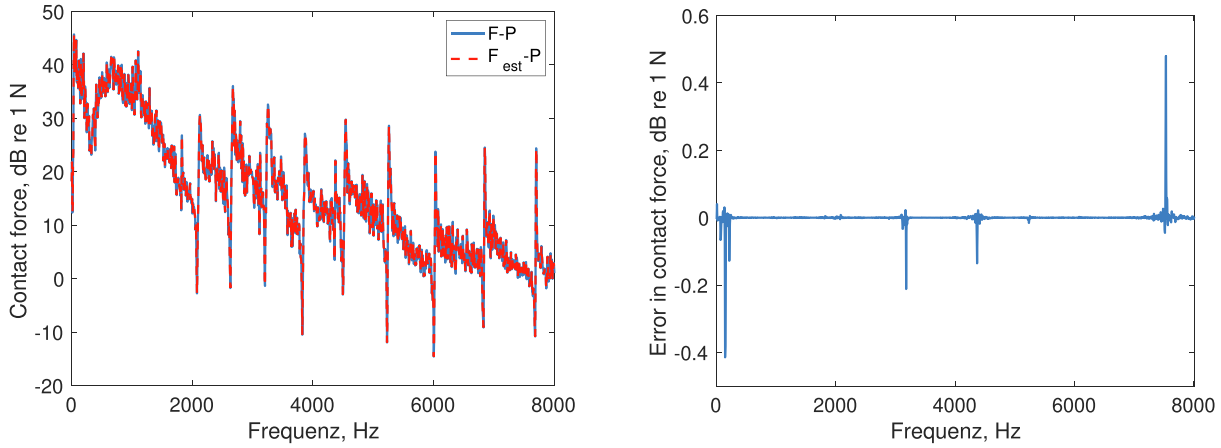

Fig. 9. Autospectrum of the original dynamic contact force $F-P$ in comparison to the estimated force $F_{\text{est}}-P$ (*left*) and error $L_{F,est}-L_F$ (*right*).

$$\mathbf{u} = \mathbf{C}\mathbf{p}, \tag{10}$$

where $\mathbf{u}$ and $\mathbf{p}$ are vectors with the entries u_e and p_e for the different elements. The matrix $\mathbf{C}$ contains the influence coefficients for the elastic half-space, e.g. found in [29]. The total contact force, F, is obtained by integrating the contact pressure over the contact area

$$F = \sum_{e=1}^{N_e} p_e \Delta x \Delta y. \tag{11}$$

The distance between the deformed wheel and rail (vector $\mathbf{d}$ with entries d_e) is obtained from

$$d_e = -\delta - r_e + z_{re} - z_{we} + u_e \tag{12}$$

in each element, where the vector $\mathbf{r} = \mathbf{r_w} - \mathbf{r_r}$ contains the combined roughness profile in the contact area, and the vectors $\mathbf{z_r}$ and $\mathbf{z_w}$ contain the profiles of the smooth rail and wheel. The contact conditions excluding adhesion ($p_e < 0$) and penetration ($d_e < 0$) are formulated as

$$\begin{aligned} d_e &\geqslant 0 \\ p_e &\geqslant 0 \\ d_e p_e &= 0\,. \end{aligned} \tag{13}$$

In WERAN, the approach of distant points is determined by the difference between wheel and rail displacement

$$\delta = \xi_{\text{w}} - \xi_{\text{r}}. \tag{14}$$

In order to use the contact model as a 3D contact filter, it is instead imposed that

$$F(\delta) = P. \tag{15}$$

The non-linear system of equations formed by (10)–(13) and (15) is then solved for the approach of distant points δ for each wheel centre position x on the rail by combining the Newton–Raphson method with an active-set strategy [18,30]. The equivalent roughness $r_{\text{eq,dir}}(x)$ is finally obtained from

$$r_{\text{eq,dir}}(x) = \delta_0 - \delta(x), \tag{16}$$

where δ_0 is the approach of distant points obtained for preload P for smooth surfaces. All calculations in this paper have been carried out with a spatial resolution of $\Delta x = \Delta y = 1\,\text{mm}$.

4.3. Results for the combined wheel/rail roughness

The spatial data of the equivalent combined wheel/rail roughness $r_{\text{eq,est}}$ estimated from the contact forces is shown in Fig. 10 in comparison to the roughness $r_{\text{eq,dir}}$ calculated directly by applying a 3D contact filter to the original roughness. Except for a small offset, the two curves appear visually almost identical. To illustrate the difference between an equivalent roughness and the original roughness profile, Fig. 10 also contains the longitudinal roughness lines of the original roughness profile.

The autospectra of the estimated and direct equivalent roughness in Fig. 11 show very good agreement, except for some discrete wavelengths, where up to 7 dB deviation occur. These discrete wavelengths correspond to the frequencies of highly undamped radial modes of the wheelset, which are the sharp *dips* in the plot of the contact force, Fig. 9 (*left*). Due to the high receptance at these frequencies, already tiny differences in the contact force not visible in Fig. 9 lead to noticeable differences in the wheel displacement, which influence the estimated roughness being in the order of micrometers. Deviations at discrete eigenfrequencies do, however, not affect the estimation of the combined roughness in 1/3-octave bands. Excellent agreement between estimated and direct equivalent roughness is seen in Fig. 12.

A good estimation of the roughness requires that the wheel position with respect to the sleepers is known. If the sleeper position is unknown, larger errors occur at the wavelengths corresponding to the sleeper passing frequency ($L_s = 0.6$ m corresponding to 37 Hz at the train speed of 80 km/h) and higher harmonics, as well as the pinned–pinned resonance (20.7 mm corresponding to 1071 Hz). The maximum deviation obtained when the sleeper position is off half a sleeper bay is shown in Fig. 13.

The correct sleeper position can, however, be identified by repeating the roughness estimation for systematically varied sleeper position. The correct sleeper position gives the lowest roughness at the sleeper passing frequency, as seen in Fig. 14.

As the position of the sleepers can be identified, it is assumed in the following that the position of the sleepers is known.

5. Separation of wheel and rail roughness

In this section, separation of wheel and rail roughness is accomplished by cycle-averaging the contact force over a distance corresponding to the wheel perimeter and performing the calculation of the roughness from the contact force separately for the part of the contact force originating from the wheel and from the rail roughness. This method [3] takes advantage of the fact that the wheel roughness is deterministic and repeats after each wheel revolution, while the rail roughness has a random character. There is, however, another contribution to the contact force, which is deterministic, too, and has not been considered in previous studies in the literature. The parametric excitation when the wheel passes over the discretely supported rail causes a deterministic contribution to the contact force that repeats with the sleeper spacing L_s.

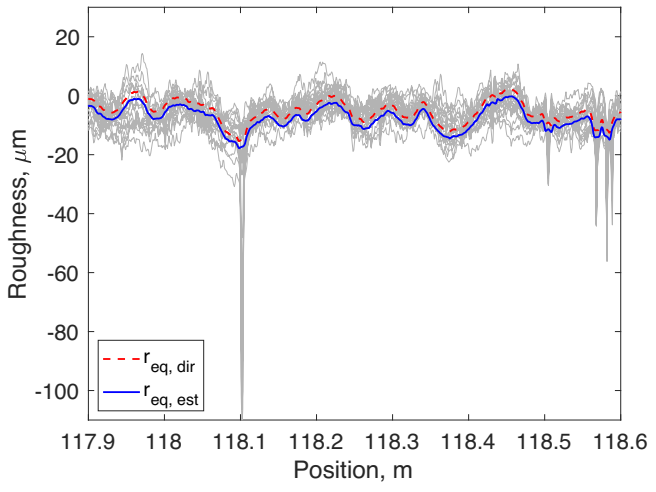

Fig. 10. Section of the equivalent combined wheel/rail roughness $r_{\mathrm{eq,est}}$ estimated from ABA in comparison to the equivalent combined roughness $r_{\mathrm{eq,dir}}$ calculated directly by applying a 3D contact filter to the original roughness. The set of original roughness lines is plotted in grey.

The following procedure has been adopted to separate wheel and rail roughness starting from the time series of the estimated contact force F_{est}:

- *Removal of sleeper influence:* The estimated force F_{est} is divided into pieces of the length of the sleeper bay, which are then averaged. This averaged force is an approximation of the part of the contact force that is generated due to parametric excitation by passing over the sleepers. The averaged force is extended to the original signal length N to give F_{s}. This signal is then removed from the estimated contact force: $F_{\mathrm{est,2}} = F_{\mathrm{est}} - F_{\mathrm{s}} + P$.
- *Determination of the part of the contact force generated by the wheel roughness:* The estimated force $F_{\mathrm{est,2}}$ is divided into pieces corresponding to the wheel perimeter, which are then averaged. The averaged force is extended to the original signal length N to give the part of the contact force generated by the wheel roughness F_{w}.
- *Addition of the sleeper effect:* $F_{\mathrm{w,2}} = F_{\mathrm{w}} + F_{\mathrm{s}} - P$.
- *Calculation of the wheel roughness:* The procedure described in Section 4.1 is applied on $F_{\mathrm{w,2}}$ to determine the equivalent wheel roughness.
- *Determination of the part of the contact force generated by the rail roughness:* The part generated by the wheel roughness is removed from the total estimated contact force to determine the part determined by the rail roughness: $F_{\mathrm{r,2}} = F_{\mathrm{est}} - F_{\mathrm{w}} + P$. (The force $F_{\mathrm{r,2}}$ already includes the sleeper effect. The part of the contact force generated purely by the rail roughness without parametric excitation is $F_{\mathrm{r}} = F_{\mathrm{r,2}} - F_{\mathrm{s}} + P$)
- *Calculation of the rail roughness:* The procedure described in Section 4.1 is applied on $F_{\mathrm{r,2}}$ to determine the equivalent rail roughness.

The sleeper effect has to be removed before cycle-averaging to determine the part of the contact force generated by the wheel roughness F_{w} and added again afterward. Otherwise, F_{w} is erroneous, and an artificial roughness is obtained at the wavelength corresponding to the sleeper passing frequency. A section of the different contributions $F_{\mathrm{s}}, F_{\mathrm{w}}$, and F_{r} to the contact force is presented in Fig. 15.

The results for separated wheel and rail roughness are shown in Fig. 16 in terms of the narrow-band autospectra and in Fig. 17 (*upper left*) and Fig. 18 in terms of the 1/3-octave band spectra and corresponding estimation error. Both wheel and rail roughness are estimated with good precision. Higher estimation errors in the rail roughness occur only where the rail roughness (due to the filtering applied to the raw data) is far below the wheel roughness, i.e. for wavelengths longer than 1 m and shorter than 5 mm. In the wavelength range 0.5 m to 5 mm, which is most relevant for rolling noise, the error is below 1 dB in all 1/3 octave bands except the one at 2 cm containing the wavelength associated with the pinned–pinned frequency, where the error is 2.6 dB. Similarly, for the wheel roughness, the error is below 1.2 dB in all bands, except one band around 25 cm, where the error reaches 2.5 dB.

In the nominal simulation case treated up to now, the equivalent rail roughness is below the equivalent wheel roughness in all 1/3-octave bands, except one. To investigate the influence of the relative amplitude of wheel and rail roughness on the success of separation, the simulation and roughness separation was repeated for a rail roughness multiplied with factors 3 and 6 while keeping the wheel roughness as previously. The results are shown in Fig. 17 (*upper right*) and (*lower*) and in Fig. 18. It is noticed that the higher the rail roughness in comparison to the wheel roughness, the higher is the error in the estimated wheel roughness. This

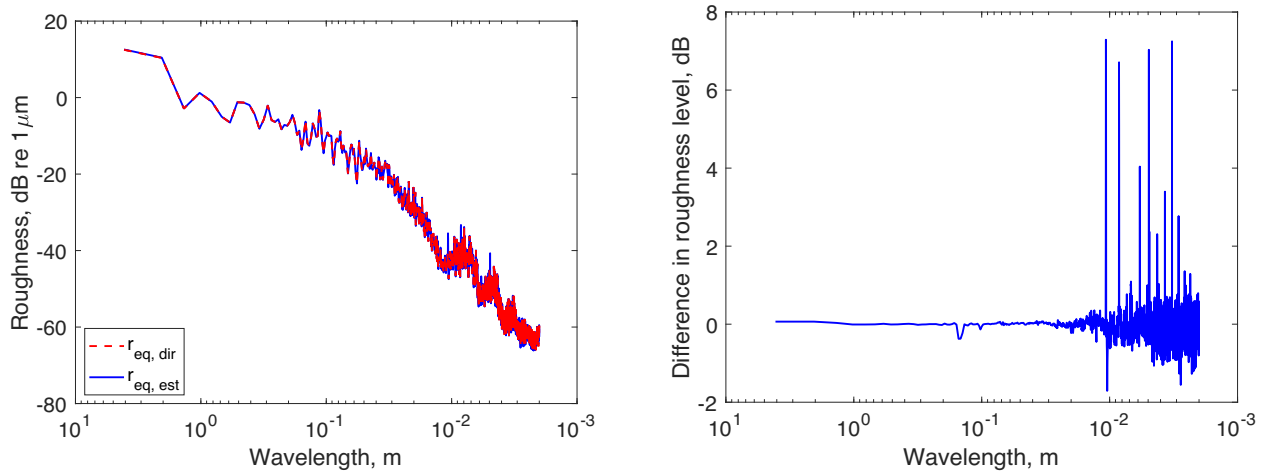

Fig. 11. Autospectrum of the equivalent combined wheel/rail roughness $r_{\mathrm{eq,est}}$ estimated from ABA in comparison to the equivalent combined roughness $r_{\mathrm{eq,dir}}$ calculated directly by applying a 3D contact filter to the original roughness (*left*) and estimation error $L_{r,\mathrm{eq,est}} - L_{r,\mathrm{eq,dir}}$ (*right*).

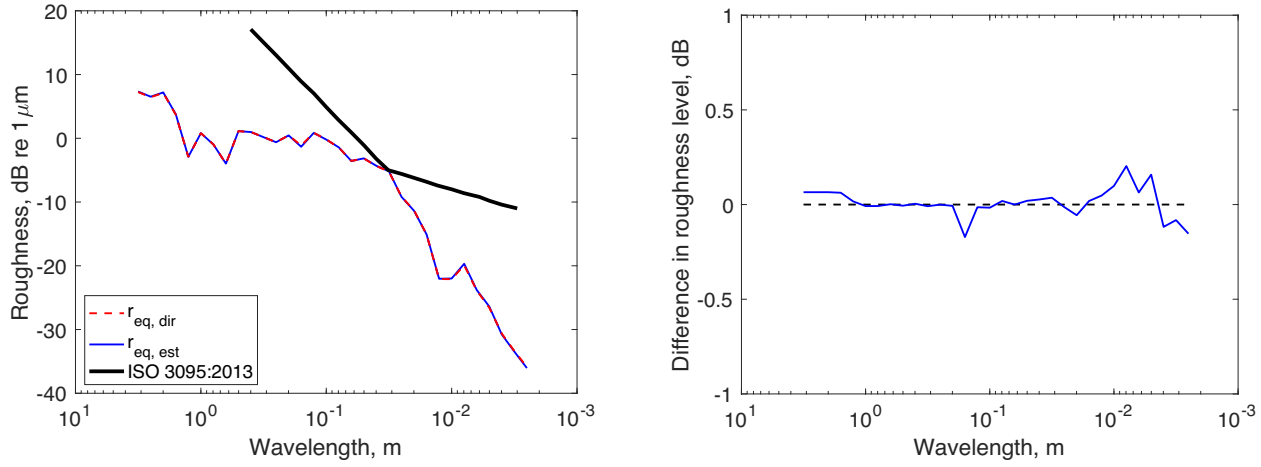

Fig. 12. 1/3-octave band spectrum of the equivalent combined wheel/rail roughness $r_{\mathrm{eq,est}}$ estimated from ABA in comparison to the equivalent combined roughness $r_{\mathrm{eq,dir}}$ calculated directly by applying a 3D contact filter to the original roughness (*left*) and estimation error $L_{r,\mathrm{eq,est}} - L_{r,\mathrm{eq,dir}}$ (*right*).

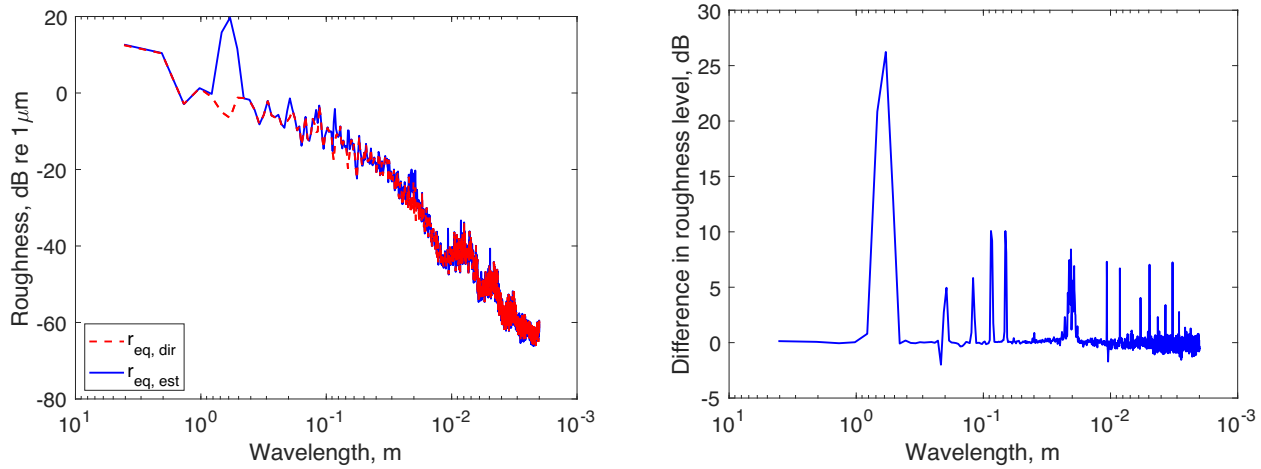

Fig. 13. Sleeper position off half a sleeper bay. Autospectrum of the equivalent combined wheel/rail roughness $r_{\mathrm{eq,est}}$ estimated from ABA in comparison to the equivalent combined roughness $r_{\mathrm{eq,dir}}$ calculated directly by applying a 3D contact filter to the original roughness (*left*) and estimation error $L_{r,\mathrm{eq,est}} - L_{r,\mathrm{eq,dir}}$ (*right*).

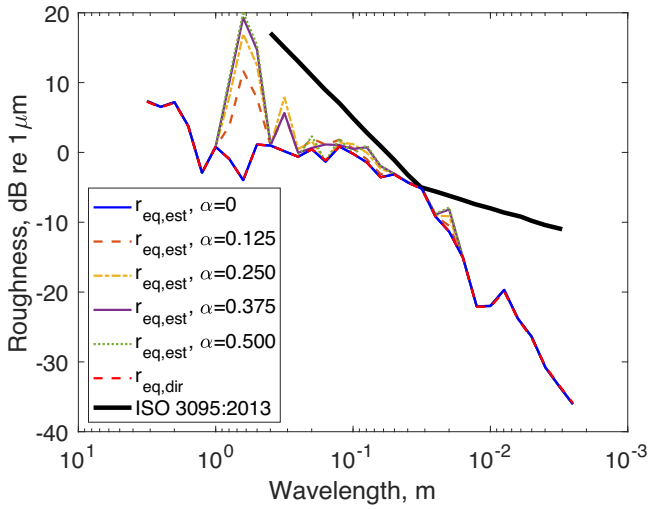

Fig. 14. 1/3-octave band spectrum of the equivalent combined wheel/rail roughness $r_{eq,est}$ estimated from ABA for a sleeper position differing from the correct position by αL_s, where L_s is the length of the sleeper bay, and 1/3-octave band spectrum of the direct equivalent roughness.

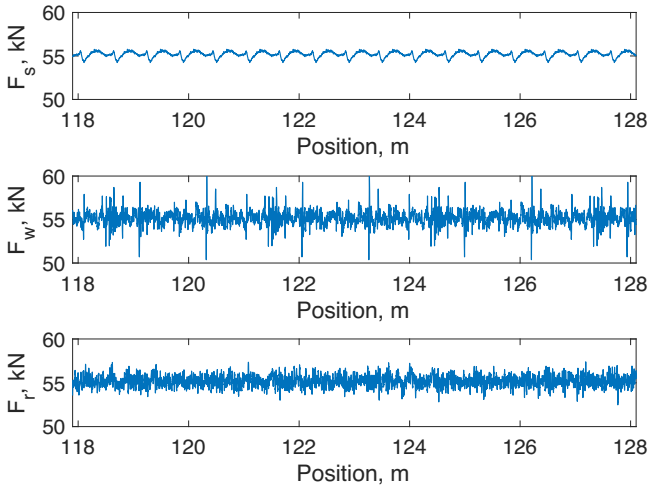

Fig. 15. Contributions to the contact force due to parametric excitation (*upper*), wheel roughness (*middle*) and rail roughness (*lower*).

is attributed to the fact that the cycle-averaging to extract the component of the contact force generated by the wheel roughness works less well when the rail roughness is dominating. This does, however, not affect the estimation of the rail roughness. On the contrary, the estimation error decreases even further when the rail roughness is increased.

6. Influence of uncertain track parameters

The contact forces generated between wheel and rail and the measured ABA signals depend on the track dynamics. This means conversely that uncertainties in the track parameters influence the precision with which wheel and rail roughness can be estimated from the ABA signal.

To investigate the precision needed in the track parameters, the identification of roughness from the ABA signal has been carried out with deliberately wrong track parameters. Fig. 19 demonstrates the error obtained in the estimated rail roughness when rail pad stiffness and damping (*left*) and ballast stiffness and damping (*right*) differ from the correct value by ±20%. Among the investigated parameters, deviations in the rail pad stiffness have the highest influence leading to up to 3.5 dB error in the mid-wavelength range, followed by the ballast damping and stiffness leading to errors up to 1.8 dB and 1.2 dB, respectively, for longer wavelengths. For the investigated deviations of ±20%, the rail pad damping only has a minor influence on the estimated rail roughness. The magnitude of the errors found for deviations in rail pad stiffness agrees well with the results by Carrigan and Talbot [6] for deviations in track support stiffness of a continuously supported rail in a similar investigation.

In practice, the rail pad stiffness may vary largely in the railway network. It does not only depend on the rail pad type but also preload [1], age [31], and temperature [32]. In this context, the presented simulation results illustrate that there is a need for a technique to extract the track parameters and in particular the rail pad stiffness from the ABA signal with high precision to be able to extract rail roughness accurately. This will be addressed in future work.

7. Conclusions

In this paper, a method to estimate spatial rail roughness data from the time series of axle box acceleration (ABA) was presented. The method is based on the time-domain model WERAN for high-frequency wheel/rail interaction and noise. Roughness estimation

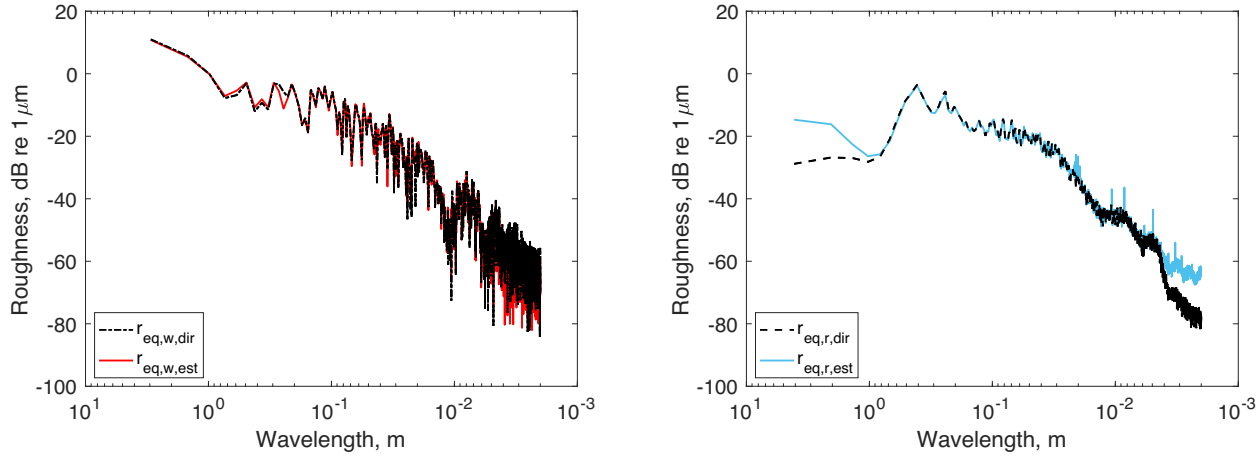

Fig. 16. Autospectrum of the equivalent wheel roughness $r_{eq,w,est}$ estimated from ABA in comparison to the equivalent wheel roughness $r_{eq,w,dir}$ calculated directly by applying a 3D contact filter to the original roughness (*left*) and corresponding plots for the rail roughness (*right*).

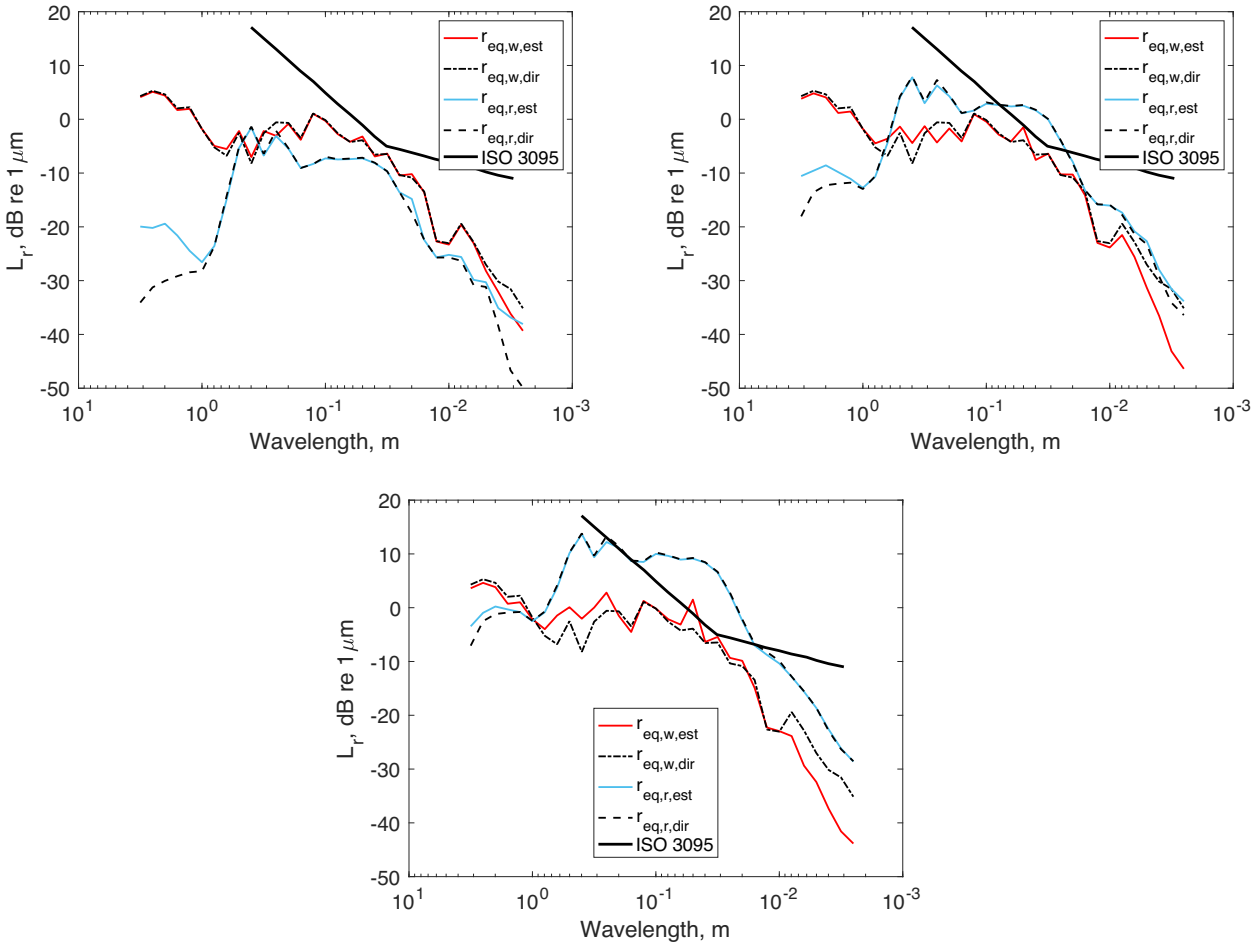

Fig. 17. 1/3-octave band spectra of the wheel and rail roughness estimated from ABA in comparison to the equivalent wheel and rail roughness calculated directly by applying a 3D contact filter to the original roughness: nominal case (*upper left*), rail roughness multiplied with factor 3 (*upper right*) and rail roughness multiplied with factor 6 (*lower*).

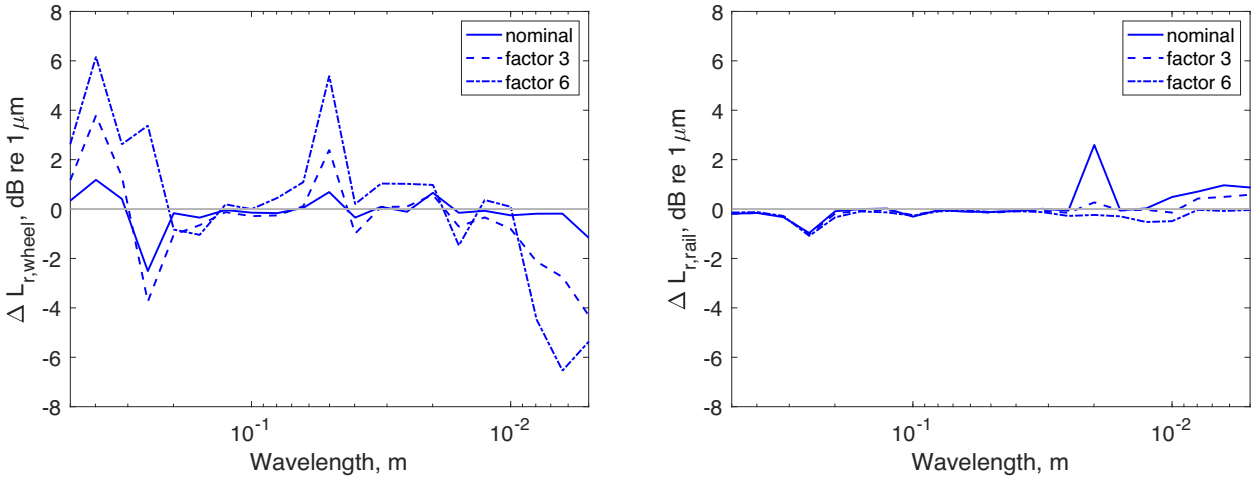

Fig. 18. Estimation error $L_{r,\mathrm{eq,est}} - L_{r,\mathrm{eq,dir}}$ for 1/3-octave band spectra of the wheel (*left*) and rail (*right*) roughness in the wavelength range 0.5 m to 5 mm.

is carried out in two steps. First, the time series of the vertical wheel/rail contact forces is derived from the ABA signal by applying an LMS algorithm for source identification. Second, the roughness is obtained from the contact force based on a non-linear Hertzian contact model and a convolutional approach to determine wheel and rail displacement. To determine wheel and rail roughness, this second step is carried out separately for the part of the contact force originating from the wheel, respectively rail roughness. The part of the contact force arising from the wheel roughness is identified by cycle-averaging the contact force over a distance corresponding to the wheel perimeter. Hereby, special attention has to be given to parametric excitation on the discretely

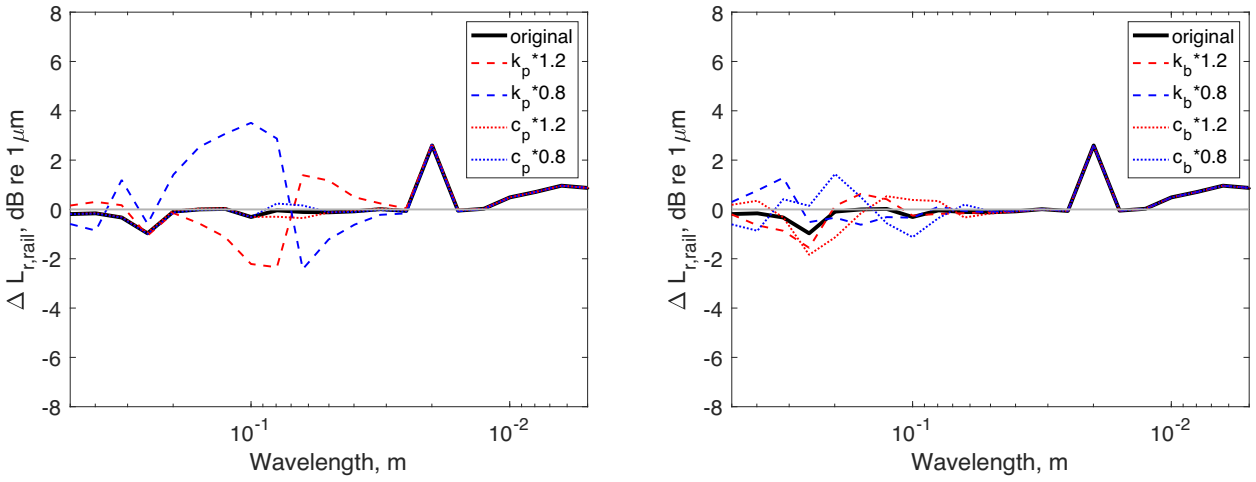

Fig. 19. Estimation error $L_{r,\mathrm{eq,est}} - L_{r,\mathrm{eq,dir}}$ for the 1/3-octave band spectra of rail roughness when track parameters differ from their actual value by $\pm 20\%$: rail pad stiffness k_p and damping c_p (*left*) and ballast stiffness k_b and damping c_b (*right*).

supported rail. To obtain the correct contribution of wheel roughness in the contact force by cycle-averaging, the sleeper effect has to be identified first and removed from the contact force. In the presented simulations, the rail roughness could be estimated with good accuracy in the relevant wavelength range from 0.5 m to 5 mm. Overall, deviations in 1/3-octave bands between estimated and actual roughness were below 1 dB. Only for low rail roughness, higher deviations of less than 2.6 dB occurred around the pinned–pinned resonance frequency. To obtain a good estimation of the rail roughness, it is important to know the position of the sleepers in relation to the registered ABA signal. In practice, it can be difficult to determine the position of the wheelset with such high precision. It has, however, been demonstrated in Section 4.3 that the position of the sleepers can be identified from the data.

In contrast to all existing methods in the literature, the presented method for rail roughness estimation is formulated in the time domain. A time-domain method requires some more computational effort than frequency-domain methods but has the advantage that the spatial variations of roughness can be detected. Although not demonstrated in this paper, this also paves the way for the detection of localized defects such as squats or deteriorated welds. The applied time-domain LMS algorithm to calculate the contact forces from the ABA signal has the advantage that it does not demand a matrix inversion leading to a more robust algorithm in the case of low signal-to-noise ratio and ill-conditioned systems. A further benefit of the time-domain approach is that parametric excitation on the discretely supported rail can be considered when estimating the roughness from the contact forces. Finally, the cycle-averaging to separate wheel and rail roughness requires to operate in the time domain. However, in a frequency domain approach, it could also be carried out on the time-domain ABA signal before switching to the frequency domain, instead of cycle-averaging the contact forces as done in this paper.

Although real measured roughness data has been used, the proposed method to estimate rail roughness has so far only been tested under ideal conditions in a simulated environment. To assess how well the method works in real conditions, it has to be investigated how much different uncertainties and noise impact the precision of the roughness estimation. This can e.g. be measurement noise or uncertainties in the transfer function from the contact point to the axle box. The position of the contact point on the wheel and rail will also vary laterally during train operation. This affects the frequency response functions of wheelset and track and which part of the roughness profile passes through the contact area. The latter will in particular influence the cycle-averaging to obtain the part of the contact force caused by the wheel roughness since this technique builds on perfect periodicity of the wheel roughness. This periodicity is impacted by a laterally meandering contact point. It has to be investigated thoroughly how limiting the lateral motion of the contact point is for the proposed method. Finally, the stiffness and damping properties of the track support have to be known. The investigation in Section 6 showed that in particular the rail pad stiffness is critical. Already relatively small deviations of 20% in rail pad stiffness lead to an error in the rail roughness of up to 3.5 dB in single 1/3-octave bands. As the track parameters vary in the railway network, it is indispensable to develop a method that simultaneously estimates both roughness and track parameters from the ABA signal.

CRediT authorship contribution statement

Astrid Pieringer: Conceptualization, Methodology, Software, Investigation, Writing – original draft, Writing – review & editing, Visualization. **Wolfgang Kropp:** Methodology, Software, Writing – review & editing.

Declaration of Competing Interest

The authors declare the following financial interests/personal relationships which may be considered as potential competing interests: Astrid Pieringer reports equipment, drugs, or supplies was provided by DB Systemtechnik GmbH. Astrid Pieringer reports a relationship with DB Systemtechnik GmbH that includes: employment.

Acknowledgements

The current study is part of the ongoing activities in CHARMEC – Chalmers Railway Mechanics (www.chalmers.se/charmec). Parts of the study have been funded from the European Union's Horizon 2020 research and innovation programme in the project In2Track2 under grant agreement No 826255. The work has also partly been funded by the Area of Advance Transport at Chalmers University of Technology in the project Intelligent railway digitization. The study also builds partly on results from the project AMONTRACK that has received funding from the European Union's Horizon 2020 research and innovation programme under the Marie Skłodowska-Curie grant agreement No 744605. We greatly

acknowledge the permission of DB Systemtechnik GmbH to use data and models from their noise measurement car. We would also like to express our gratitude to Dr.Giacomo Squicciarini from ISVR, University of Southampton, for providing the measured rail roughness data and the measured wheel and track frequency response functions used in this study.

References

[1] Thompson D. Railway noise and vibration: Mechanisms, modelling and means of control. 1st ed. Oxford, UK: Elsevier; 2009.
[2] Spänner J. A new approach of assessing rail roughness. In Proceedings of the 4th International Conference on Railway Condition Monitoring, Derby, UK; 2008.
[3] Németh I, Schleinzer G. Investigation into the indirect determination of wheel-rail surface roughness. In: Proceedings of the 11th Mini Conference on Vehicle System Dynamics. Budapest: Identification and anomalies; 2008. p. 135–46.
[4] Bocciolone M, Caprioli A, Cigida A, Collina A. A measurement system for quick rail inspection and effective track maintenance strategy. Mech Syst Signal Process 2007;21:1242–54.
[5] Bongini E, Grassie S, Saxon M. 'Noise mapping' of a railway network: Validation and use of a system based on measurement of axlebox vibration. In: Maeda T et al., editors. Noise and Vibration Mitigation for Rail Transportation Systems. Notes on Numerical Fluid Mechanics and Multidisciplinary Design, vol. 118. Tokyo: Springer; 2012. p. 505–13.
[6] Carrigan T, Talbot J. Extracting information from axle-box accelerometers: on the derivation of rail roughness spectra in the presence of wheel roughness. In: G. Degrande, et al. (Eds.), Noise and Vibration Mitigation for Rail Transportation Systems, Vol. 150 of Notes on Numerical Fluid Mechanics and Multidisciplinary Design, Springer Cham; 2021. pp. 286–294.
[7] Asmussen B, Onnich H, Strube R, Greven L, Schröder S, Jäger K, Degen K. Status and perspectives of the "specially monitored track. J Sound Vib 2006;293:1070–7.
[8] Jones R, Packham A. Acoustic monitoring of rail-head roughness for targeted grinding and noise modelling. In: 2006 IET International Conference on Railway Condition Monitoring, Birmigham, UK. p. 61–2.
[9] Kuijpers AHWM. Rail roughness monitoring in the Netherlands. In: B. Schulte-Werning, et al. (Eds.), Noise and Vibration Mitigation for Rail Transportation Systems, Vol. 99 of Notes on Numerical Fluid Mechanics and Multidisciplinary Design, Springer Verlag Berlin Heidelberg; 2008. pp. 348–354.
[10] Kuijpers AHWM, Schwanen W, Bongini E. Indirect rail roughness measurement: The ARRoW system within the LECAV project. In: Maeda T et al., editors. Noise and Vibration Mitigation for Rail Transportation Systems. Notes on Numerical Fluid Mechanics and Multidisciplinary Design, vol. 118. Tokyo: Springer; 2012. p. 563–70.
[11] Chartrain P-E. Lecture acoustique de la voie ferrée [Ph.D. thesis]. Université d'Aix-Marseille, France; 2013.
[12] Tufano AR, Chiello O, Pallas MA, Faure B, Chaufour C, Augez R, Reynaud E, Vincent N. Calibration of transfer functions on a standstill vehicle for on-board indirect measurements of rail acoustic roughness, in: Proceedings of Forum Acusticum 2020, Lyon, France; 2020.
[13] Tufano AR, Chiello O, Pallas M-A, Faure B, Chaufour C, Reynaud E, Vincent N. Numerical and experimental analysis of transfer functions for on-board indirect measurements of rail acoustic roughness. In G. Degrande, et al. (Eds.), Noise and Vibration Mitigation for Rail Transportation Systems, Vol. 150 of Notes on Numerical Fluid Mechanics and Multidisciplinary Design, Springer Cham; 2021. pp. 295–302.
[14] Pallas M-A, Tufano A-R, Chiello O. Separation of rail and wheel roughness from on-board vibroacoustic measurements. In: Proceedings of Forum Acusticum 2020, Lyon, France; 2020.
[15] Pieringer A, Kropp W, Nielsen J. The influence of contact modelling on simulated wheel/rail interaction due to wheel flats. Wear 2014;314(1–2):273–81.
[16] Widrow B, Hoff ME. Adaptive switching circuits. In 1960 IRE WESCON Convention Record, Part 4, New York; 1960. pp. 96–104.
[17] Pieringer A. A numerical investigation of curve squeal in the case of constant wheel/rail friction. J Sound Vib 2014;333(18):4295–313.
[18] Kalker JJ. Three-Dimensional Elastic Bodies in Rolling Contact. Dordrecht, Boston, London: Kluwer Academic Publishers; 1990.
[19] Maglio M, Pieringer A, Nielsen J, Vernersson T. Wheel–rail impact loads and axle bending stress simulated for generic distributions and shapes of discrete wheel tread damage. J Sound Vib 2021;502:116085.
[20] Thompson D, Squicciarini G, Zhang J, Lopez Arteaga I, Zea E, Dittrich M, Jansen E, Arcas K, Cierco E, Magrans FX, Malkoun A, Iturritxa E, Guiral A, Stangl M, Schleinzer G, Martin Lopez B, Chaufour C, Wändell J. Assessment of measurement-based methods for separating wheel and track contributions to railway rolling noise. Appl Acoust 2018;140:48–62.
[21] Nielsen J, Igeland A. Vertical dynamic interaction between train and track – influence of wheel and track imperfections. J Sound Vib 1995;187(5):825–39.
[22] Pieringer A, Stangl M, Rothhämel J, Tielkes T. Acoustic monitoring of rail faults in the German railway network. In G. Degrande, et al. (Eds.), Noise and Vibration Mitigation for Rail Transportation Systems, Vol. 150 of Notes on Numerical Fluid Mechanics and Multidisciplinary Design, Springer Cham; 2021. pp. 242–250.
[23] CEN. Railway applications – noise emission – rail roughness measurement related to noise generation, European standard EN 15610:2009; 2009.
[24] CEN. Railway applications – measurement of noise emitted by railbound vehicles, Standard ISO 3095:2013; 2013.
[25] Thompson D. On the relationship between wheel and rail surface roughness and rolling noise. J Sound Vib 1996;193(1):149–60.
[26] Pieringer A, Kropp W, Thompson D. Investigation of the dynamic contact filter effect in vertical wheel/rail interaction using a 2D and a 3D non-Hertzian contact model. Wear 2011;271:328–38.
[27] Kropp W, Larsson K. Force estimation in the time domain by applying an LMS-algorithm. In Proceedings of Noise and Vibration: Emerging Methods (NOVEM) 2005, St. Raphaël, France; 2005.
[28] Kropp W, Larsson K, Lobato T, Sottek R. Application of the LMS algorithm to identify the surface velocity responsible for the radiated sound pressure. Acta Acust 5(32).
[29] Johnson K. Contact mechanics. first paperback edition. Cambridge University Press; 1987.
[30] Pieringer A. Time-domain modelling of high-frequency wheel/rail interaction [Ph.D. thesis]. Chalmers University of Technology: Gothenburg, Sweden; 2011.
[31] Oregui M, de Man A, Woldekidan M, Li Z, Dollevoet R. Obtaining railpad properties via dynamic mechanical analysis. J Sound Vib 2016;363:460–72.
[32] Squicciarini G, Thompson DJ, Toward M, Cottrell RA. The effect of temperature on railway rolling noise. Proc Inst Mech Eng Part F 2016;230(8):1777–89.